EFFECT OF THE METHOD OF COMPACTION ON THE KINETICS OF FORMATION OF THE PORE SPACE STRUCTURE AND THE PHYSICOMECHANICAL PROPERTIES OF ARTIFICIAL STONE

M. F. Kazanskii, B. Z. Dragunskii,
V. M. Kazanskii, R. V. Lutsyk,
and N. M. Minenko

UDC 666.972

The kinetics of formation of the pore space structure of artificial stone and its differential water-retaining and physicomechanical properties have been comprehensively investigated with allowance for the effect of the method of compaction.

It has been established that the various methods of compacting concrete mixes do not all have the same effect on the mechanical properties and permeability of the matured material. This is a result of their effect on the formation of the microstructure (the structure of artificial stone).

We have investigated the effect of vibration (frequency 60 cps, amplitude 0.35 mm), vibrocompression (frequency 60 cps, amplitude 0.35 mm, pressure $3 \cdot 10^6$ N/m^2), and centrifugation (compacting pressure $2 \cdot 10^5$ N/m^2) on the hydration kinetics, the formation of the mechanical structure of the pore space, and certain physicomechanical properties of artificial stone based on Portland cement M600, supplied by the Zdolbunovskii Plant, at $(W/C)_r = K = 0.26$.

The hydration kinetics were investigated by thermogravimetric analysis using a Paulik (Hungary) derivatograph system. For each specimen at specified curing times we recorded a thermogram, a weight curve, and a curve showing the rate of change of weight (derivatogram).

In order to study the kinetics of formation of the structural porosity we employed the method of drying thermograms [1], which was shown to be appreciable under conditions similar to ours in [2]. The structure of the pore space of the matured material was also investigated by low- and high-pressure mercury porometry.

In parallel tests we determined the compressive and bending strengths and the nitrogen permeability at a pressure of 10^6 N/m^2. At individual stages of the curing process we determined the microhardness and the specific surface from the water vapor and nitrogen adsorption (BET).

In Fig. 1 we have reproduced the general appearance of the drying thermograms for each specimen; it is possible to distinguish a number of critical points corresponding to evaporation limits: an excess of free moisture above the specimen (up to point 1), capillary moisture from the macropores and the intergranular space (from point 1 to point 2); meniscus moisture from the macropores of the intergranular space and the pores of the artificial stone grains with a radius $10^{-7} < r < 2 \cdot 10^{-5}$ m (from point 2 to point 3); moisture contained in the microcapillaries of the artificial stone with a radius $5 \cdot 10^{-9} < r < 10^{-7}$ m (from point 3 to point 4); polymolecular adsorption moisture in pores with a radius $1 \cdot 10^{-9} < r < 5 \cdot 10^{-9}$ m (from point 4 to point 5); monomolecular adsorption moisture in pores with a radius $4 \cdot 10^{-10} < r < 1 \cdot 10^{-9}$ m (from point 5 to point 6); and, finally, moisture retained in the artificial stone by weak chemical forces (beyond point 6) [3].

Kiev Technological Institute of Light Industry. Translated from Inzhenerno-Fizicheskii Zhurnal, Vol. 21, No. 4, pp. 681-687, October, 1971. Original article submitted January 8, 1971.

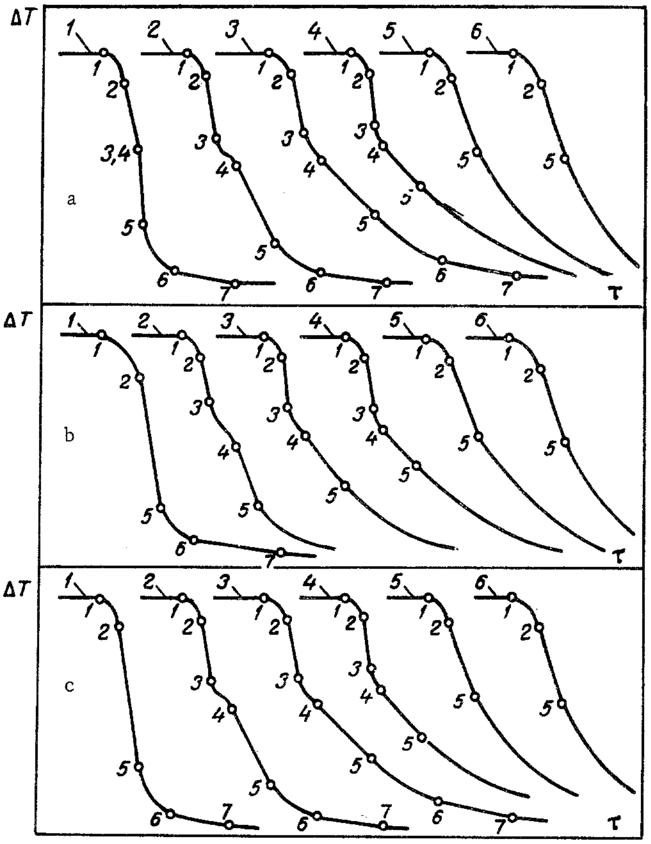

Fig. 1. Typical drying thermograms of specimens I (a), IV (b), and V (c) at the ages: 1) 3 h; 2) 8 days; 3) 28 days; 4) 6 months; 5) 1 year; 6) 1.5 years. ΔT is the specimen–air temperature difference, °K; τ is the duration of the experiment, sec.

Thus the moisture contents of the specimen at the critical points on the thermogram (points 2, 3, 4, 5, 6) are of special importance in connection with the investigation of the structural porosity [2].

The drying thermograms of the vibrocompacted material (specimen I) are presented in Fig. 1a. On the first thermogram, recorded 3 h after mixing, the critical points 3 and 4 coincide, which indicates the absence of detectable microcapillaries in the initial period of formation of the coagulation–crystallization structure. Then the relative location of the critical points on the thermogram is observed to change, and points 3 and 4 separate. After 8 days the thermogram takes a form generally typical of brittle gels (curve 2 in Fig. 1a). After 28 days the segment between points 3 and 4 gradually contracts, which is associated with a decrease in the volume of the micropores as a result of their being overgrown by submicrocrystalline hydration products. Subsequently, the shapes of the thermograms and the locations of the critical points remain unchanged. On the thermograms recorded up to 28 days after mixing it is possible to distinguish a critical point 6, which indicates the presence of a certain amount of moisture weakly bound by chemical forces.

The evolution of the thermogram for vibrocompressed material (specimen IV) is shown in Fig. 1b and that of the thermogram for centrifuged artificial stone (specimen V) in Fig. 1c. In general, the form of the thermograms is the same as for specimen I, except that points 6 and 7 are less easily distinguishable on the thermograms obtained for specimen IV.

The changes in the shape of the thermograms only qualitatively characterize the kinetics of pore structure formation. Quantitative information was obtained by analyzing the numerical values of the moisture content at each critical point on thermograms recorded during the curing process.

In Fig. 2 we have plotted the changes in the volume of macro-, micro-, and submicroporosity in specimens I, IV, and V calculated with respect to unit mass of artificial stone dried at 378°K. All the

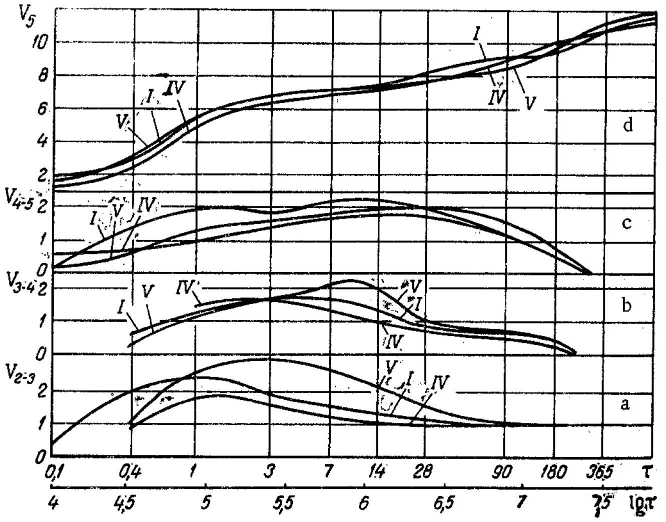

Fig. 2. Macropore volume $V_{2-3}(\cdot 10^{-5}\ m^3/kg)$ (a), micropore volume $V_{3-4}(\cdot 10^{-5}\ m^3/kg)$ (b), gel pore volume $V_{4-5}(\cdot 10^{-5}\ m^3/kg)$ (c), and monolayer adsorption volume $V_5(\cdot 10^{-5}\ m^3/kg)$ (d) as functions of the curing time τ (days) and $\log\tau$ (sec) for specimens I, IV, and V.

curves were constructed on the assumption that irrespective of pore size the density of the water is equal to $10^3\ kg/m^3$.

The method of compaction has its greatest effect on the differential characteristic of the pore space during the first 1-4 days, i.e., during the period of most active formation and consolidation of the crystallization framework.

Subsequently (after 3-4 days from the time of mixing) during the curing of all the forms of artificial stone considered there is a fall in macropore volume ($2\cdot 10^{-5} > r > 10^{-7}$ m) owing to an increase in the volume of new hydrated formations. This explains the rapid growth of the gel submicropore volume (Fig. 2c, d) and the micropore volume (Fig. 2b). The increase in the number of micropores during the initial period of curing is also caused by the contraction compression of the volume of the primary gel structure.

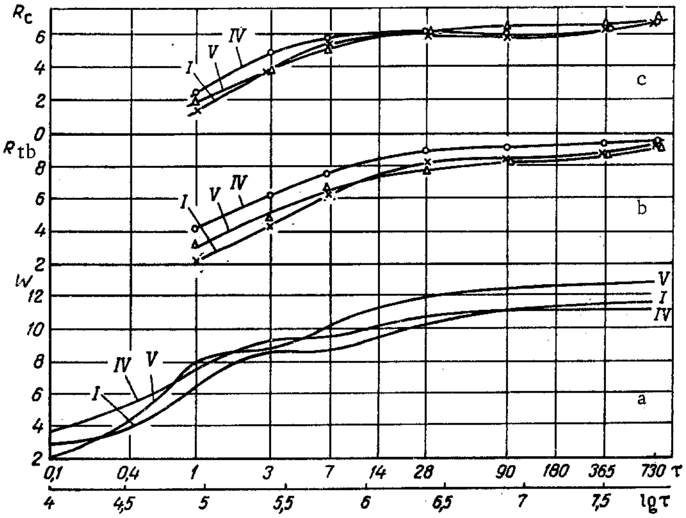

Fig. 3. Amount of water of hydration W_h (%) (a), tensile bending strength $R_{tb}(\cdot 10^6\ N/m^2)$ (b), and compressive strength $R_c(\cdot 10^7\ N/m^2)$ (c) as functions of the curing time τ (days) for specimens I, IV, and V.

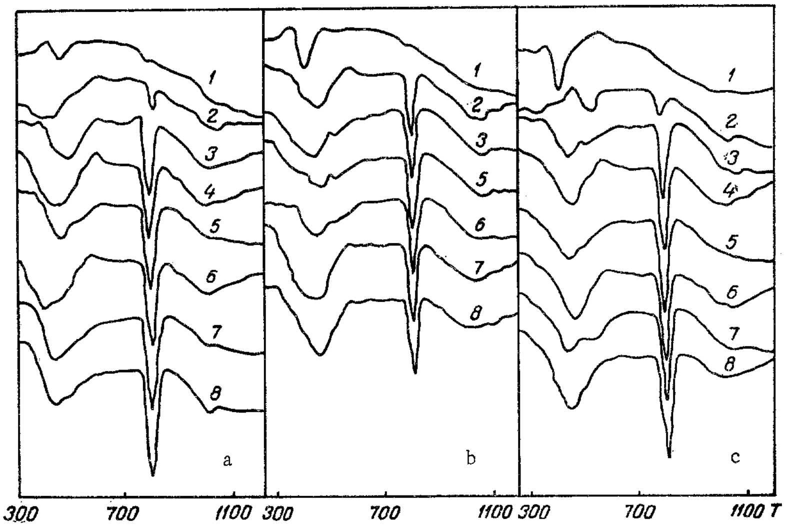

Fig. 4. Derivatograms of specimens I (a), IV (b), and V (c) at the ages of 3 h (1), 8 h (2), 1 day (3), 2 days (4), 3 days (5), 7 days (6), 14 days (7), and 28 days (8). T is temperature, °K.

Compression during the compaction process and the initial period of curing (during the setting phase) ensures the densest packing of the solid-phase particles, expulsion of air, and intense structure formation in the vibrocompressed artificial stone.

From the very beginning of curing under normally moist conditions the vibrocompressed material (specimen IV, Fig. 2a) has the least macrocapillary pore volume at similar relative micro- and submicropore volumes (Fig. 2b, c, d).

The high degree of hydration of specimen IV in the initial curing period is graphically illustrated by the curves representing the changes in moisture of hydration (Fig. 3a) and by the characteristic peaks corresponding to the formation of calcium hydroxide on the derivatograms (Fig. 4).

At the end of the first day the compressive and bending strengths of the vibrocompressed material are almost twice as great as the corresponding strengths of the vibrocompacted specimens (Fig. 3b, c).

This sharp difference in the mechanical properties of material compacted in different ways during the initial curing period is confirmed by the results of a determination of the microvolume cohesion strength or microhardness. After three days the values were 1.4, 1.7, and $2.7 \cdot 10^6$ N/m^2 for vibrocompacted, centrifuged, and vibrocompressed artificial stone, respectively.

One of the properties of artificial stone most closely related with its structural porosity parameters is its gas permeability. The permeability coefficient directly characterizes the filtration qualities of the material. At a pressure of 10^6 N/m^2 pores with a radius greater than 10^{-7} m are permeable to nitrogen.

Thanks to its denser structure after three days vibrocompressed artificial stone has a gas permeability coefficient 2.5 orders lower than that of the vibrocompated material and one order lower than that of the centrifuged stone (Table 1).

The fact that the gas permeability of the centrifuged material subsequently approaches that of the vibrocompacted stone has the following explanation. Although it somewhat intensifies structure formation in the early stages, nonetheless the pressure acting during the centrifugal compaction process creates a

TABLE 1. Gas Permeability of Artificial Stone

Method of compaction	Gas permeability coefficient (darcy) when tested at age(days):				
	3	7	28	360	550
Vibration	$2 \cdot 10^{-2}$	$1 \cdot 10^{-3}$	$7 \cdot 10^{-4}$	$9 \cdot 10^{-5}$	$6 \cdot 10^{-5}$
Vibrocompression	$8 \cdot 10^{-4}$	$7 \cdot 10^{-5}$	$3 \cdot 10^{-5}$	$9 \cdot 10^{-6}$	$7 \cdot 10^{-6}$
Centrifugation	$7 \cdot 10^{-3}$	$2 \cdot 10^{-3}$	$9 \cdot 10^{-4}$	$2 \cdot 10^{-4}$	$9 \cdot 10^{-5}$

directional capillarity, so-called filtration channels. In reality, during the first month of curing the centrifuged specimen has the most developed micropore structure.

The difference in the structure of the pore space of specimens I, IV, and V at the age of one month (according to the data on moisture content difference and the mercury porometry data) is also responsible for the difference in the gas permeabilities. The differences in microhardness (4.6, 4.2, and $6.5 \cdot 10^6$ N/m^2) and in tensile bending strength (7.2, 7.8, and $9.5 \cdot 10^6$ N/m^2) are also preserved.

At this point, according to the mercury porometry data, the pore radius at the distribution maximum is 4.62, 5.00, and $3.25 \cdot 10^{-8}$ m for the vibrated, centrifuged, and vibrocompressed specimens, respectively. At the end of the first month the compressive strength, the functional relation of which with the differential pore characteristic is less distinctly expressed, is almost independent of the method of compaction (see Fig. 3).

An investigation of the variation of the pore space structure and certain physicomechanical characteristics of the artificial stone during the process of further curing (up to 1.5 years) reveals a trend toward a leveling off of the effect of the method of compaction on the properties in question.

After 18 months of normally moist curing the investigated specimens have almost equal volumes occupied by gel submicropores, which is attributable, on the one hand, to the earlier stabilization of the development of these pores in the vibrocompressed material and, on the other, to the continued development of the gel pores in the structures of the vibrated and centrifuged stones. The volumes occupied by macro- and micropores in the investigated specimens also tend to converge. The equal degree of hydration in specimens compacted by different methods is confirmed by the results of the thermographic (Fig. 3a) and derivatographic (Fig. 4) analyses.

At eighteen months neither the compressive strength nor the tensile bending strength depend on the compaction technique. The gas permeabilities, determined by the number and shape of the filtering capillaries, converge for the centrifuged and vibrated material, and that of the vibrocompressed stone is less than one order different (Table 1).

The convergence of the parameters of the pore space structure of the various types of artificial stone is confirmed by the experimental data on the specific surface of the solid phase. After two years the specific surface, determined from the nitrogen and water adsorption, is independent of the method of compaction and has the values $(5.2 \pm 0.5) \cdot 10^3$ m^2/kg for nitrogen and $(22.0 \pm 1.0) \cdot 10^3$ m^2/kg for water.

The difference in the absolute values of the specific surface determined by different methods is attributable to the nonuniqueness of the water vapor and nitrogen adsorption mechanisms [4, 5].

After two years all the specimens have almost the same microhardness (6.8, 6.4, and $6.9 \cdot 10^6$ N/m^2).

Thus, in the early stages of cure the kinetics of structure formation and the physicomechanical properties of artificial stone are to a considerable extent determined by the method of compaction. In the later stages of cure there is a tendency for the principal structural parameters and the material properties to converge.

LITERATURE CITED

1. M. F. Kazanskii, Dokl. Akad. Nauk SSSR, 130, No. 5, 1059 (1960).
2. M. F. Kazanskii and V. M. Kazanskii, in: The Problem of Heat and Mass Transfer [in Russian], Énergiya (1970).
3. V. M. Kazanskii, Inzh.-Fiz. Zh., 15, No. 6, 1027 (1968).
4. O. P. Mtschedlow-Petrossian and D. A. Uginschus, Silikattechnik, 20, No. 12, 416 (1969).
5. T. Feneĉ and S. Seza, Epitöanyag, 21, No. 3, 90 (1969).